Supporting Information

Reversing C_2H_2–CO_2 adsorption selectivity in an ultramicroporous metal–organic framework platform

Hui-Min Wen,[a] Caijun Liao,[a] Libo Li,[b,c] Ling Yang,[c] Jing Wang,[a] Liang Huang,[a] Bin Li,*[d] Banglin Chen*[b] and Jun Hu*[a]

[a] College of Chemical Engineering, Zhejiang University of Technology, Zhejiang, 310014, P. R. China. E-mail: hjzjut@zjut.edu.cn

[b] Department of Chemistry, University of Texas at San Antonio, One UTSA Circle, San Antonio, Texas 78249-0698, USA. Fax: (+1)-210-458-7428. E-mail: banglin.chen@utsa.edu

[c] College of Chemistry and Chemical Engineering, Taiyuan University of Technology, Taiyuan 030024, Shanxi, P. R. China

[d] State Key Laboratory of Silicon Materials, School of Materials Science and Engineering, Zhejiang University, Hangzhou, 310027. E-mail: bin.li@zju.edu.cn

Experimental Section

1. General Procedures and Materials. All starting reagents and solvents were purchased from commercial companies and used without further purification. Powder X–ray diffraction (PXRD) patterns were measured by a Rigaku Ultima IV diffractometer operated at 40 kV and 44 mA with a scan rate of 2 deg min^{-1}. C_2H_2 (99.99%), CO_2 (99.99%), He (99.999%) and C_2H_2/CO_2 = 50/50 (v/v) gas mixtures were purchased from Beijing Special Gas Co. LTD (China).

Synthesis of $[Ni(pyz–SH)_2(SiF_6)]_n$ (ZJUT-2). The powder samples of ZJUT-2 were synthesized using the same methods of SIFSIX-3-Ni and its amino analogues $[Ni(pyz–NH_2)_2(SiF_6)]_n$ (ZJUT-1) reported in the corresponding literatures.[1,2] ZJUT-2 was synthesized by the solvothermal reaction of nickel hexafluorosilicate ($NiSiF_6$, 1 mmol) with 2-thiolpyrazine (pyz-SH, 2 mmol) in 20 mL methanol at 85 ^oC. A light blue powder was obtained after 3 days, collected by filtration and then washed with methanol (61% yield based on pyz-SH). The phase purity of the bulk material was confirmed by PXRD.

2. Powder X-ray Crystallography. Attempts to obtain single crystals for single-crystal X-ray diffraction measurement were not successful. We thus relied on powder X-ray diffraction (PXRD) to confirm the high purity of the powder sample and to simulate the crystallographic structure.[2-4] The PXRD measurements were performed on a Rigaku Ultima IV diffractometer, operated at 40 kV and 44 mA and CuKα radiation (λ = 1.5406 Å). Data were collected at room temperature in the 2θ range of 2−45° with a step size of 0.5°. We first indexed the PXRD pattern and identified a monoclinic *C2* space group. Then, based on the framework connection of SIFSIX-3-Ni, we built a crystal structure model for ZJUT-2. The orientation of pyrazine rings was optimized to avoid the space overlapping and collision of -SH groups with circumjacent atoms. The -SH groups were modeled as fully ordered in the structure (Fig. S1). In reality, there might exist some orientational disorder associated with the -SH groups. The simulated PXRD pattern of our structural model agrees excellently with the experimental data (Fig. S3, ESI†), strongly supporting its validity. Some structural information of ZJUT-2 is provided in Tables S1 and S2.

3. Gas sorption measurements. A Micromeritics ASAP 2020 surface area analyzer was used to measure gas adsorption isotherms. To remove all the guest solvents in the framework, the fresh powder samples were first solvent-exchanged with dry methanol at least 10 times within two days,

and evacuated at room temperature (298 K) for 24 h and additional 12 h at 323 K until the outgas rate was 5 mmHg min^{-1} prior to measurements. The sorption measurement was maintained at 196 K under dry ice-acetone bath. An ice-water bath (slush) and water bath were used for adsorption isotherms at 273 and 296 K, respectively.

4. Breakthrough experiments. The breakthrough curves of ZJUT-2a were measured on a homemade apparatus for gases mixtures C_2H_2/CO_2 (50/50) at 298 K and 1.0 bar. In the separation experiment, ZJUT-2a (0.7045 g) particles with diameters of 200-300 μm were prepared and packed into Φ 4 × 60 mm stainless steel column, and the column was activated under reduced pressure at 323 K overnight. The experimental set-up consisted of two fixed-bed stainless steel reactors. One reactor was loaded with the adsorbent, while the other reactor was used as a blank control group to stabilize the gas flow. The gas flows were controlled at the inlet by a mass flow meter as 2 mL/min, and a gas chromatograph (TCD-Thermal Conductivity Detector, detection limit 0.1 ppm) continuously monitored the effluent gas from the adsorption bed. Prior to every breakthrough experiment, we activated the sample by flushing the adsorption bed with helium gas for 2 hours at 373 K. Subsequently, the column was allowed to equilibrate at the measurement rate before we switched the gas flow.

5. Virial Graph Analysis

Estimation of the isosteric heats of gas adsorption (Q_{st})

A virial-type expression of comprising the temperature-independent parameters a_i and b_j was employed to calculate the enthalpies of adsorption for C_2H_2 and CO_2 (at 273 K and 296 K) on ZJUT-2a, respectively. In each case, the data were fitted use equation:

$$\ln P = \ln N + 1/T \sum_{i=0}^{m} a_i N_i + \sum_{j=0}^{n} b_j N_j \qquad (1)$$

Here, P is the pressure expressed in Pa, N is the amount absorbed in mmol g^{-1}, T is the temperature in K, a_i and b_j are virial coefficients, and m, n represent the number of coefficients required to adequately describe the isotherms (m and n were gradually increased till the contribution of extra added a and b coefficients was deemed to be statistically insignificant towards the overall fit. And the average value of the squared deviations from the experimental values was minimized). The

values of the virial coefficients a_0 through a_m were then used to calculate the isosteric heat of absorption using the following expression:

$$Q_{st} = -R\sum_{i=0}^{m} a_i N_i \quad (2)$$

Q_{st} is the coverage-dependent isosteric heat of adsorption and R is the universal gas constant. The heat enthalpy of C_2H_2 and CO_2 sorption for complex ZJUT-2a in this manuscript are determined by using the sorption data measured in the pressure range from 0-1 bar (at 273 K and 296 K).

6. IAST calculations of adsorption selectivities

The selectivity of preferential adsorption of component *1* over component *2* in a mixture containing *1* and *2*, can be formally defined as:

$$S_{ads} = \frac{q_1/q_2}{p_1/p_2} \quad (3)$$

In equation (3), q_1 and q_2 are the absolute component loadings of the adsorbed phase in the mixture. These component loadings are also termed the uptake capacities. We calculate the values of q_1 and q_2 using the Ideal Adsorbed Solution Theory (IAST) of Myers and Prausnitz.

7. Fitting of pure component isotherms

Experimental data on pure component isotherms for C_2H_2 and CO_2 in ZJUT-2a were measured at 296 and 273 K. The pure component isotherm data for C_2H_2 and CO_2 were fitted with the Dual site Langmuir-Freundlich (DSLF) model:

$$N = N_1^{\max}\frac{b_1 p^{1/n1}}{1+b_1 p^{1/n1}} + N_2^{\max}\frac{b_2 p^{1/n2}}{1+b_2 p^{1/n2}} \quad (4)$$

where p (unit: Kpa) is the pressure of the bulk gas at equilibrium with the adsorbed phase, N (unit: mol/Kg) is the adsorbed amount per mass of adsorbent, N_1^{max} and N_2^{max} (unit: mol/Kg) are the saturation capacities of sites 1 and 2, b_1 and b_2 (unit: 1/kPa) are the affinity coefficients of sites 1 and 2, and n_1 and n_2 represent the deviations from an ideal homogeneous surface. Here, the single-component C_3H_4 and C_3H_6 adsorption isotherms have been fit to enable the application of IAST in simulating the performance of ZJUT-1a under a mixed component gas. Adsorption isotherms and gas selectivity calculated by IAST for 50/50 C_2H_2/CO_2 (v/v) mixtures in the ZJUT-2a.

8. GCMC simulations

All the GCMC simulations were performed in the MS modeling.[5] The crystal structures of SIFSIX-3-Ni and ZJUT-2a were chosen for related simulations without further geometry optimization. The framework and the individual C_2H_2 and CO_2 molecules were considered to be rigid during the simulation. Partial charges for atoms of guest-free SIFSIX-3-Ni and ZJUT-2a were derived from QEq method and QEq_neutral1.0 parameter. The simulations were carried out at 298 K, adopting the locate task, Metropolis method in Sorption module and the universal force field (UFF). The partial charges on the atoms of C_2H_2 (C: −0.129e; H1: 0.129e, where e = 1.6022×10^{-19} C is the elementary charge) and CO_2 (C: 0.894e; O: −0.447e) were also derived from QEq method. The interaction energy between hydrocarbon molecules and framework were computed through the Coulomb and Lennard-Jones 6-12 (LJ) potentials. The cutoff radius was chosen as 12.5 Å for the LJ potential and the long-range electrostatic interactions were handled using the Ewald & Group summation method. The loading steps and the equilibration steps were 1×10^5, the production steps were 1×10^6**.** The binding energy between the framework and gas molecule was then calculated using: $\Delta E = E_{(MOF)} + E_{(gas)} - E_{(MOF+gas)}$.

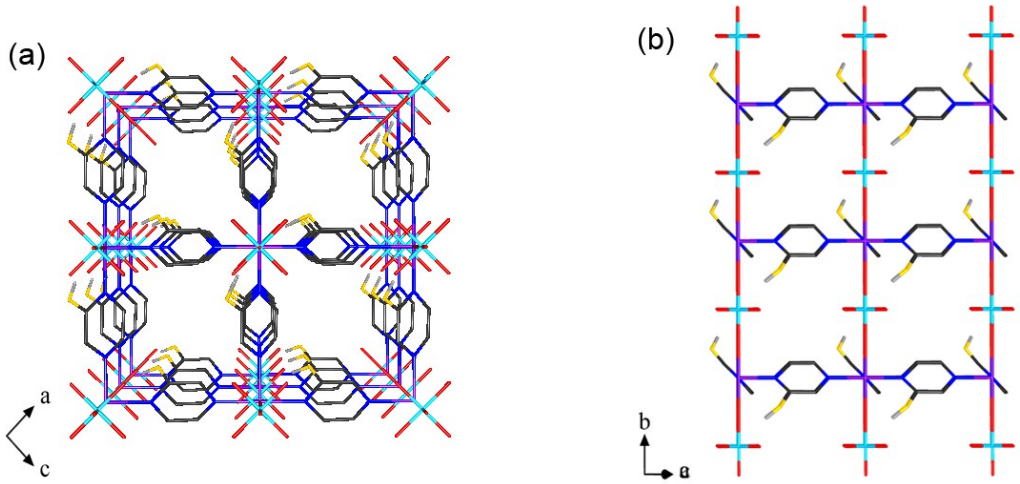

Figure S1. Illustration of the model structures of ZJUT-2, viewed along *b*-axis and *c*-axis, respectively.

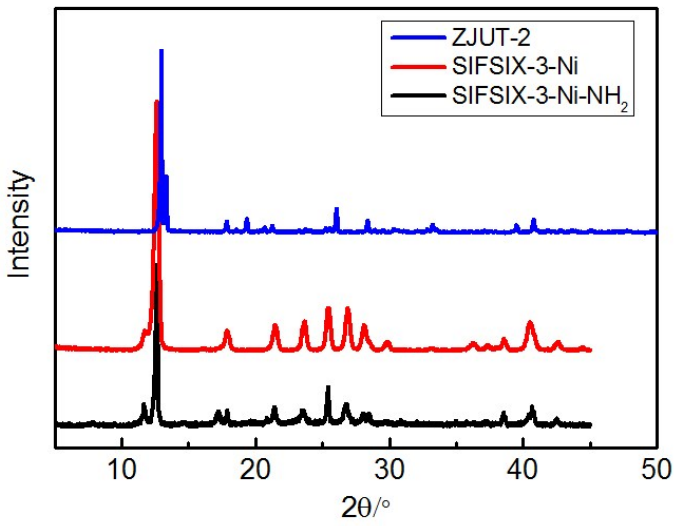

Figure S2. Experimental PXRD patterns of as-synthesized ZJUT-2, SIFSIX-3-Ni and its amino analogues SIFSIX-3-Ni-NH_2 (also called ZJUT-1), all of which match well with each other.

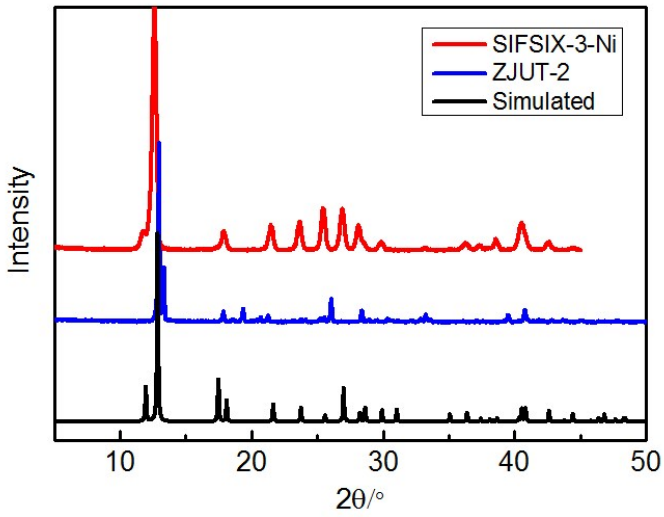

Figure S3. PXRD patterns of as-synthesized ZJUT-2 (blue) and SIFSIX-3-Ni (red) compared with the calculated XRD pattern from the structure of ZJUT-2 (black), confirming that the structure of ZJUT-2 is isoreticular to the nets of SIFSIX-3-Ni.

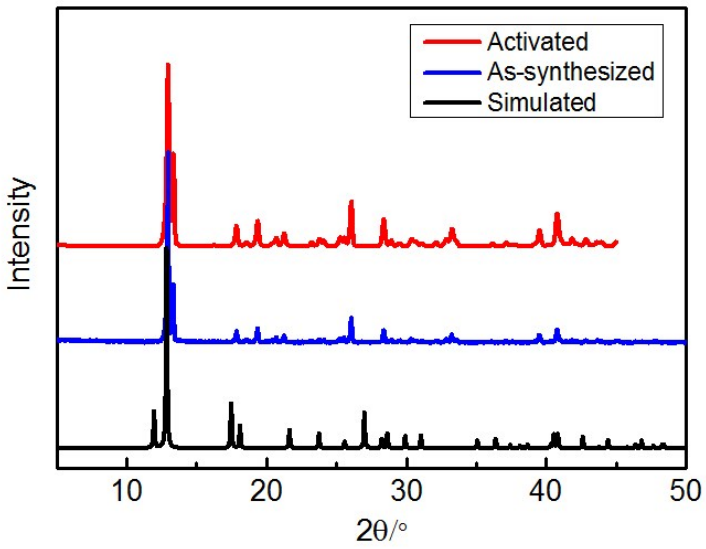

Figure S4. PXRD patterns of as-synthesized ZJUT-2 (blue) and activated ZJUT-2a (red) along with the calculated XRD pattern from the model structure of ZJUT-2 (black).

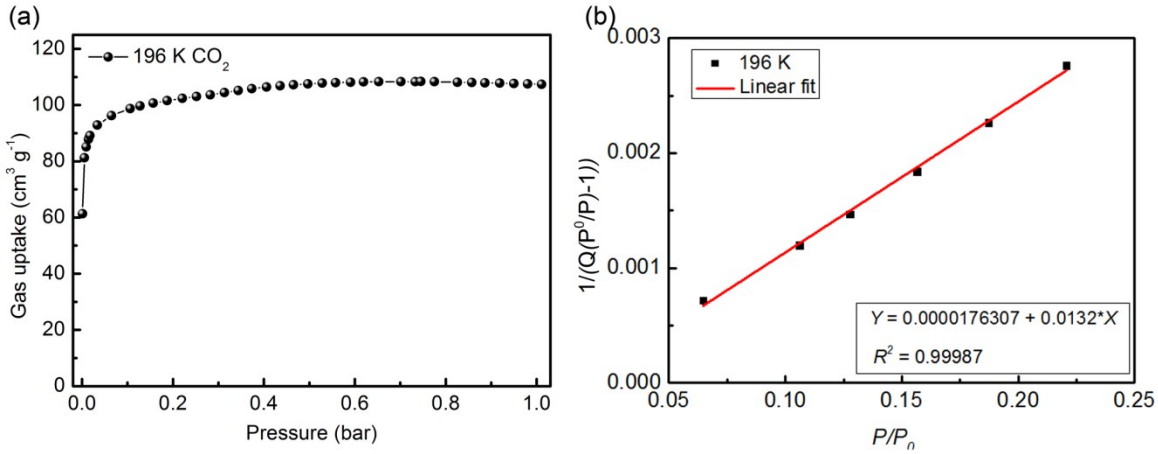

$$S_{BET} = (1/(0.0132 - 1.76307 \times 10^{-4}))/22414 \times 6.023 \times 10^{23} \times 0.170 \times 10^{-18} = 350\ m^2\ g^{-1}$$

Figure S5. (a) Gas adsorption isotherms of ZJUT-2a for CO_2 at 196 K, and the BET surface area of ZJUT-2a obtained from the 196 K CO_2 isotherms, which is slightly lower than that of SIFSIX-3-Ni reported (368 $m^2\ g^{-1}$).

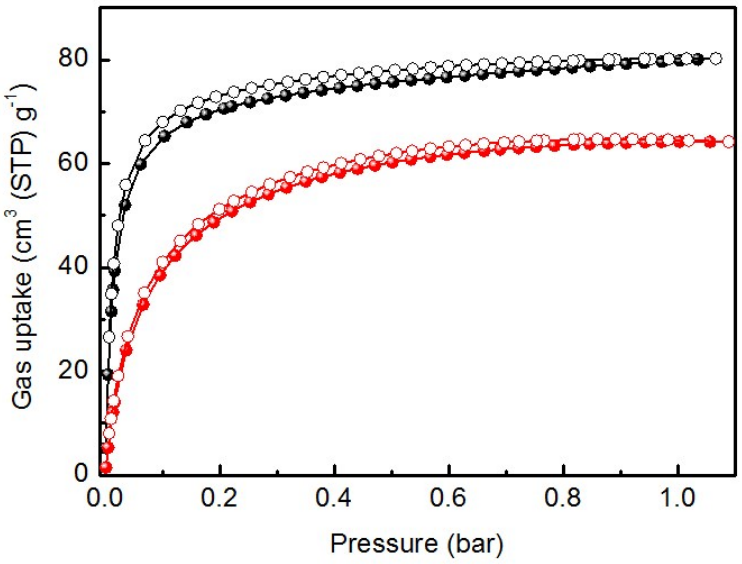

Figure S6. Adsorption isotherms of C_2H_2 (black) and CO_2 (red) for ZJUT-2a at 273 K up to 1 bar. Filled/empty circles represent adsorption/desorption.

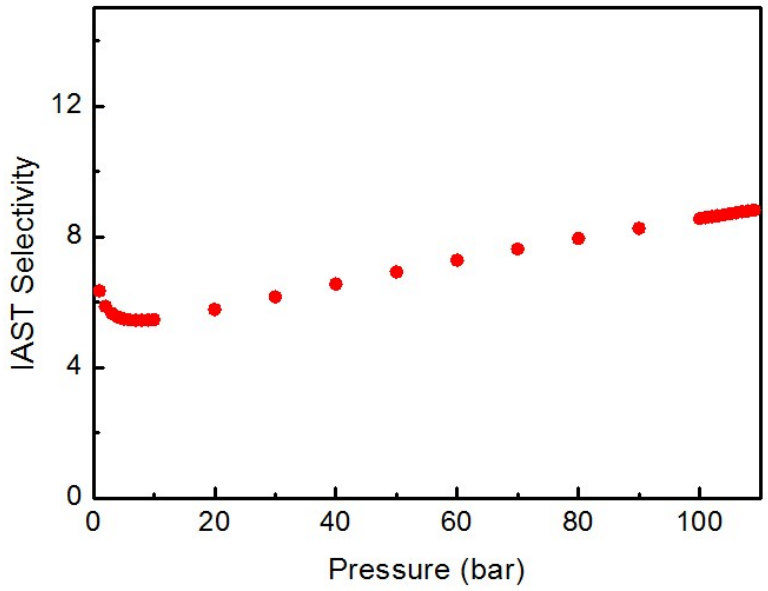

Figure S7. IAST selectivity of ZJUT-2a for C_2H_2/CO_2 (50/50, v/v) at 296 K.

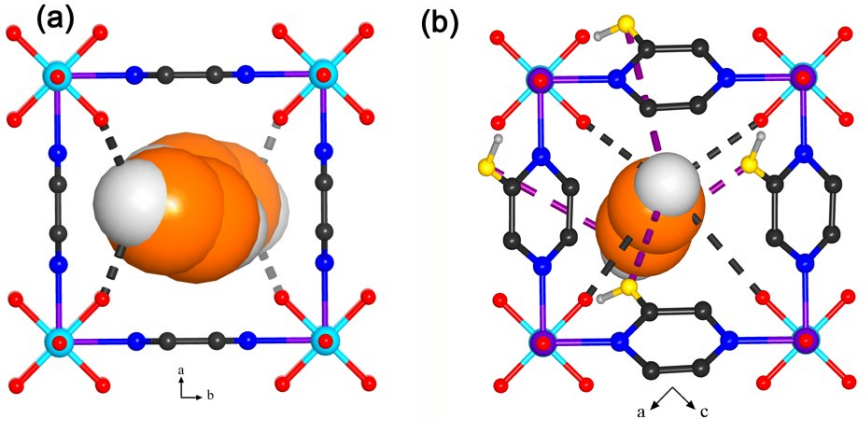

Figure S8. The calculated C_2H_2 adsorption binding sites in the cage of SIFSIX-3-Ni (a) and ZJUT-2a (b) viewed along *c*- and *b*-axis, respectively, clearly indicating that these two MOFs have notably distinct binding sites toward C_2H_2 molecule.

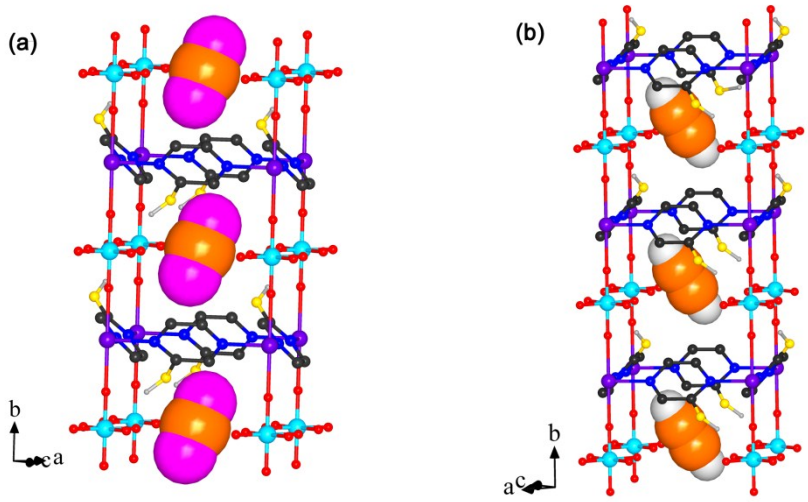

Figure S9. The calculated (a) CO_2 and (b) C_2H_2 adsorption binding sites in the nanocage of ZJUT-2a, clearly indicating that one unit can trap a single CO_2 or C_2H_2 molecule due to the contracted cage sizes and –SH functionalities.

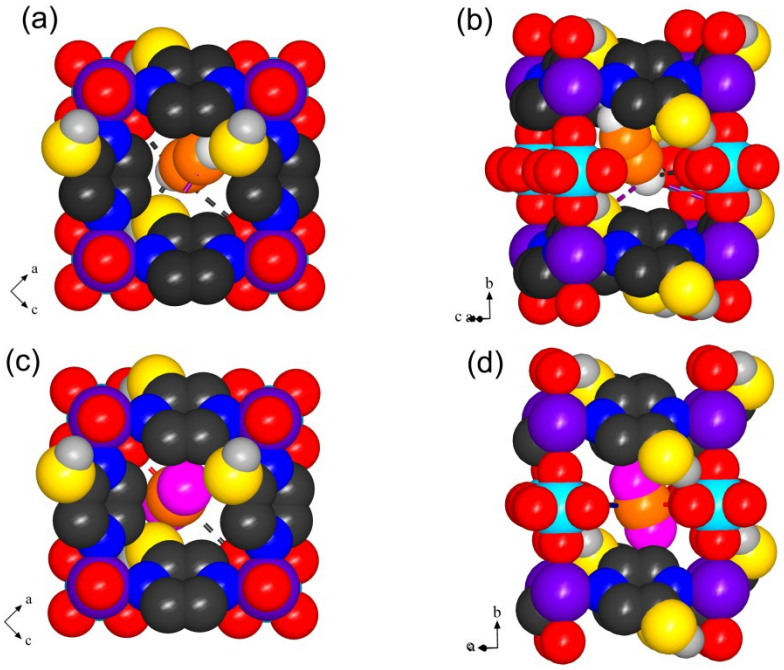

Figure S10. View of the framework-gas interaction in ZJUT-2a after adding vdw radius for all the atoms: (a and b) for C_2H_2 molecule; (c and d) for CO_2 molecule.

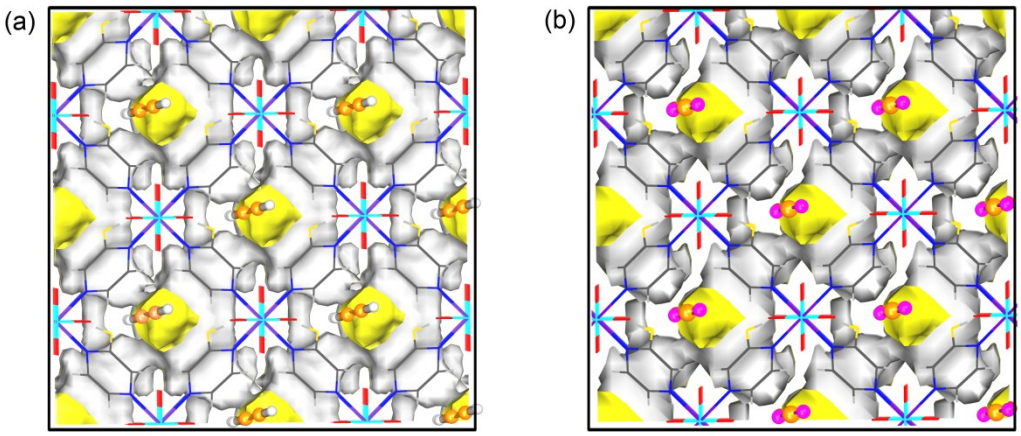

Figure S11. The Connolly surface of ZJUT-2a with the guest C_2H_2 (a) and CO_2 (b) molecules viewed along the *b*-axis (probe radius 0.9 Å).

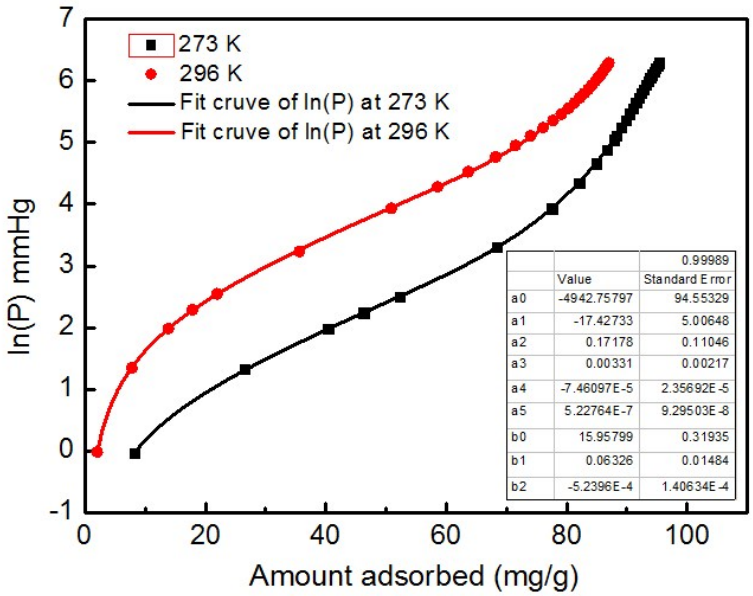

Figure S12. Virial fitting of the C_2H_2 adsorption isotherms for ZJUT-2a.

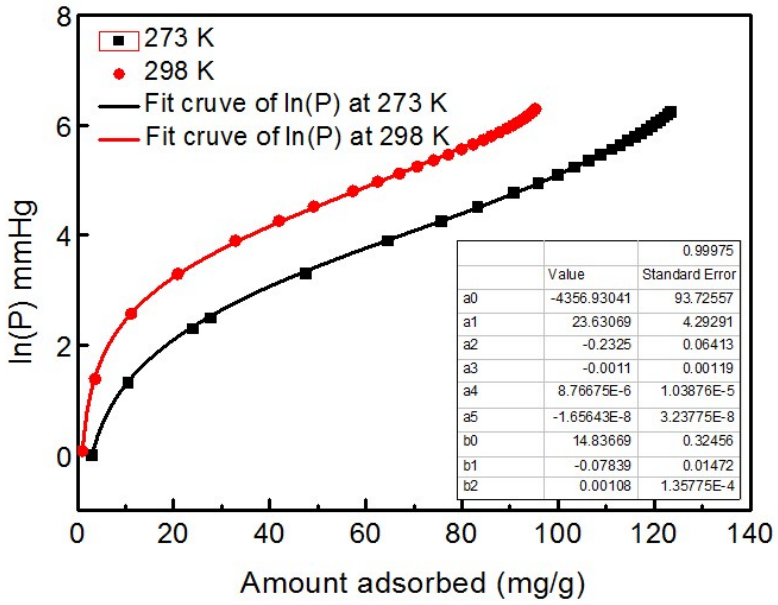

Figure S13. Virial fitting of the CO_2 adsorption isotherms for ZJUT-2a.

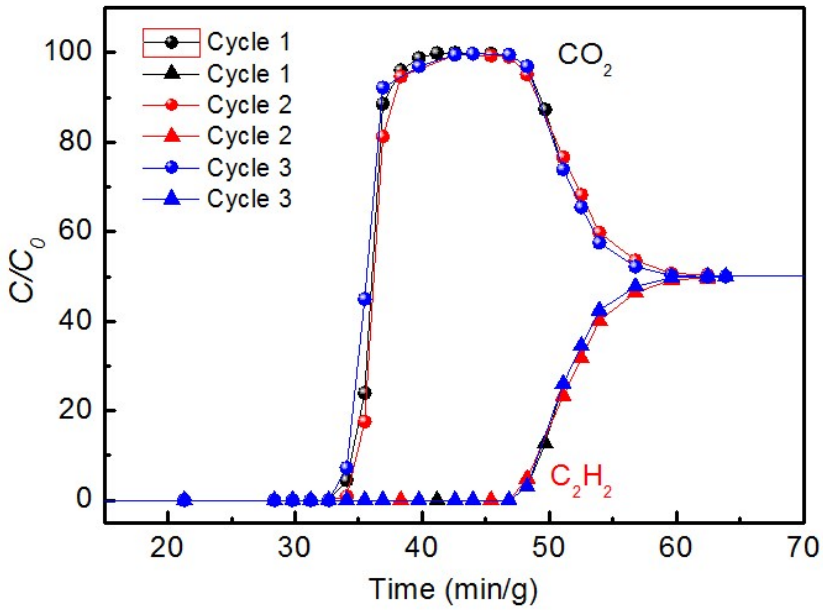

Figure S14. Cycling column breakthrough curves for C_2H_2/CO_2 separation (50/50, v/v) with ZJUT-2a at 298 K and 1.0 bar. The breakthrough experiments were carried out in a column packed with ZJUT-2a (Φ 4.0 × 60 mm) at a flow rate of 2 mL/min.

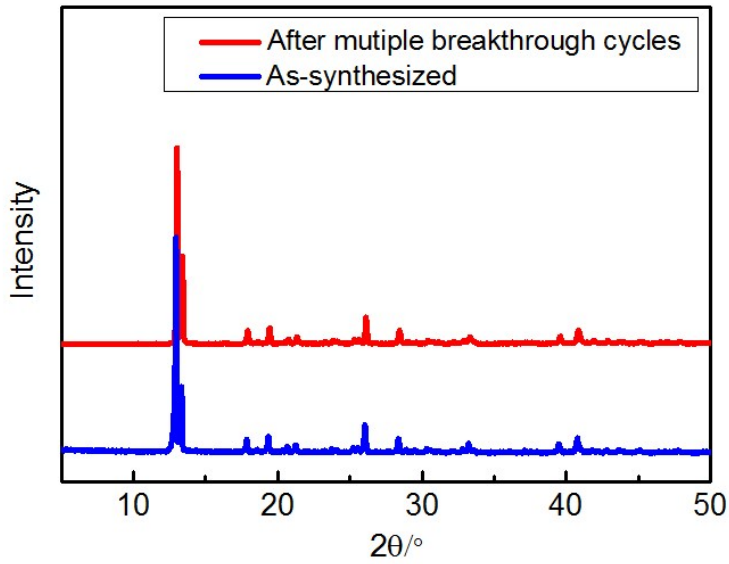

Figure S15. PXRD patterns of as-synthesized ZJUT-2 sample (blue) and the samples after the multiple breakthrough tests (red), indicating its good recyclability for C_2H_2/CO_2 separation.

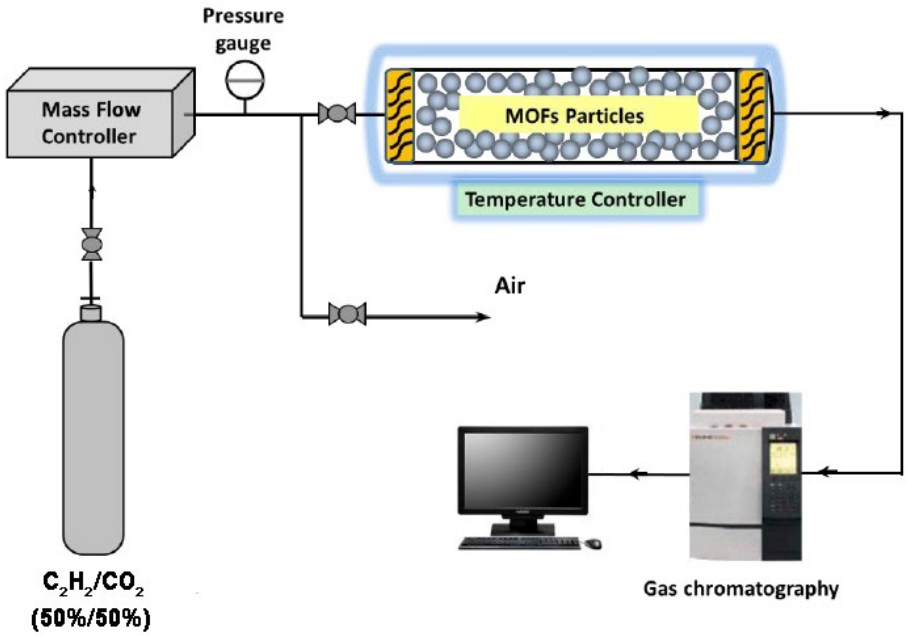

Breakthrough experiments apparatus

Figure S16. Schematic illustration of the apparatus for the breakthrough experiments.

Table S1. Lattice parameters of the modeled structure of ZJUT-2.

Unit cell parameters	ZJUT-2
Formula	$C_8H_8NiF_6N_4S_2Si$
Formula weight	425.08
Crystal system	Monoclinic
Space group	*C2*
a, *c* (Å)	9.9363
b (Å)	7.5660
α (°)	90.00
β (°)	90.00
γ (°)	90.00
V (Å^3)	746.992
Z	2
D_{calcd} (g cm^{-3})	1.890

Note: the -SH groups were modeled as fully ordered in the structure. In reality, there might exist some orientational disorder associated with the -SH groups.

Table S2. List of atomic coordinates for the modeled structure of ZJUT-2.

Atoms	x	y	z	s.o.f.
H1	0.30808	0.79196	0.02959	1.00
H2	0.42838	0.31857	0.25432	1.00
H3	0.07058	0.68250	0.25041	1.00
H4	0.25013	0.32091	0.42094	1.00
C5	0.24092	0.60293	0.14721	1.00
C6	0.35047	0.39149	0.26020	1.00
C7	0.13809	0.60474	0.24725	1.00
C8	0.25145	0.39082	0.35062	1.00
S9	0.23113	0.71065	0.06042	1.00
N10	0.35455	0.50000	0.14545	1.00
N11	0.14545	0.50000	0.35455	1.00
F12	0.33740	0.00000	0.00000	1.00
F13	0.50000	0.20810	0.00000	1.00
F14	0.50000	0.00000	-0.16260	1.00
F15	0.50000	0.00000	0.16260	1.00
Si16	0.50000	0.00000	0.00000	1.00
Ni17	0.50000	0.50000	0.00000	1.00

Table S3. Comparison of the gas uptake and selectivity of ZJUT-2 and some selected promising MOFs for C_2H_2/CO_2 (50/50, v/v) separation.

C_2H_2-selective MOFs	C_2H_2 uptake[a] (cm^3/g)	Selectivity[b]	$Q_{st,C2H2}$ (KJ/mol)	CO_2-selective MOFs	CO_2 uptake[a] (cm^3/g)	Selectivity[b]	$Q_{st,CO2}$ (KJ/mol)
ZJUT-2a	**76**	**10**	**41.5**	Mn(bdc)(dpe)[13]	46.8[c]	8.8[c]	30
NKMOF-1-Ni[6]	61.0	249.3	60.3	CD-MOF-2[14]	59	16.0	67.2
UTSA-74[7]	104	9	31	SIFSIX-3-Ni[10]	60	7.7	50.9
DICRO-4-Ni-i[8]	43	13.9	37.7				
JCM-1[9]	75	13.8	36.9				
TIFSIX-2-Cu-i[10]	4.1	6.5	46.3				
FJU-90[11]	180	4.3	25.1				
Zn-MOF-74[7]	122	3	43.8				
ZJU-40[12]	216	11.5	34.5				

[a]At 1 bar and room temperature; [b]IAST selectivity at 1 bar and room temperature; [c]At 273 K.

References

[1] S. K. Elsaidi, M. H. Mohamed, H. T. Schaef, A. Kumar, M. Lusi, T. Pham, K. A. Forrest, B. Space, W. Xu, G. J. Halder, J. Liu, M. J. Zaworotko and P. K. Thallapally, *Chem. Commun.*, **2015**, *51*, 15530.

[2] H.-M. Wen, L. Li, R.-B. Lin, B. Li, B. Hu, W. Zhou, J. Hu and B. Chen, *J. Mater. Chem. A*, **2018**, *6*, 6931.

[3] G. Xu, B. Li, H. Wu, W. Zhou and B. Chen, *Cryst. Growth Des.*, **2017**, *17*, 4795.

[4] H. Li, L. Li, R.-B. Lin, G. Ramirez, W. Zhou, R. Krishna, Z. Zhang, S. Xiang and B. Chen, *ACS Sustainable Chem. Eng.*, **2019**, *7*, 4897.

[5] *Accelrys*, Materials Studio Getting Started, release 5.0, Accelrys Software, Inc., San Diego, CA, **2009**.

[6] Y. L. Peng, T. Pham, P. Li, T. Wang, Y. Chen, K. J. Chen, K. A. Forrest, B. Space, P. Cheng, M. J. Zaworotko and Z. Zhang, *Angew. Chem. Int. Ed.*, **2018**, *57*, 10971.

[7] F. Luo, C. Yan, L. Dang, R. Krishna, W. Zhou, H. Wu, X. Dong, Y. Han, T.-L. Hu, M. O'Keeffe, L. Wang, M. Luo, R.-B. Lin and B. Chen, *J. Am. Chem. Soc.*, **2016**, *138*, 5678.

[8] H. S. Scott, M. Shivanna, A. Bajpai, D. G. Madden, K.-J. Chen, T. Pham, K. A. Forrest, A. Hogan, B. Space, J. J. Perry IV and M. J. Zaworotko, *ACS Appl. Mater. Interfaces*, **2017**, *9*,

33395.

[9] J. Lee, C. Y. Chuah, J. Kim, Y. Kim, N. Ko, Y. Seo, K. Kim, T. H. Bae and E. Lee, *Angew. Chem. Int. Ed.*, **2018**, *57*, 7869.

[10] K.-J. Chen, H. S. Scott, D. G. Madden, T. Pham, A. Kumar, A. Bajpai, M. Lusi, K. A. Forrest, B. Space, J. J. Perry and M. J. Zaworotko, *Chem*, **2016**, *1*, 753.

[11] Y. Ye, Z. Ma, R.-B. Lin, R. Krishna, W. Zhou, Q. Lin, Z. Zhang, S. Xiang and B. Chen, *J. Am. Chem. Soc.*, **2019**, *141*, 4130.

[12] H.-M. Wen, H. Wang, B. Li, Y. Cui, H. Wang, G. Qian and B. Chen, *Inorg. Chem.*, **2016**, *55*, 7214.

[13] M. L. Foo, R. Matsuda, Y. Hijikata, R. Krishna, H. Sato, S. Horike, A. Hori, J. Duan, Y. Sato, Y. Kubota, M. Takata and S. Kitagawa, *J. Am. Chem. Soc.*, **2016**, *138*, 3022.

[14] L. Li, J. Wang, Z. Zhang, Q. Yang, Y. Yang, B. Su, Z. Bao and Q. Ren, *ACS Appl. Mater. Interfaces*, **2019**, *11*, 2543.